Achieving type-II SnSSe/as van der waals heterostructure with satisfactory oxygen tolerance for optoelectronic and photovoltaic applications

Yee Hui Robin Chang, Junke Jiang, Keat Hoe Yeoh, Yusuf Zuntu Abdullahi, Heng Yen Khong, Moi Hua Tuh, Fui Kiew Liew, Yit Lian Liew

Credit Author Statement

Y.H.R. Chang: Conceptualization, Methodology, Software, Formal analysis, Investigation, Data curation, Project administration, Writing - original draft. J. Jiang, K.H. Yeoh: Software, Formal analysis, Investigation, Validation, Resources, Writing - review & editing. H.Y. Khong, Y.Z. Abdullahi, M.H. Tuh, F.K. Liew, Y.L. Liew: Validation, Visualization, Writing - review & editing.

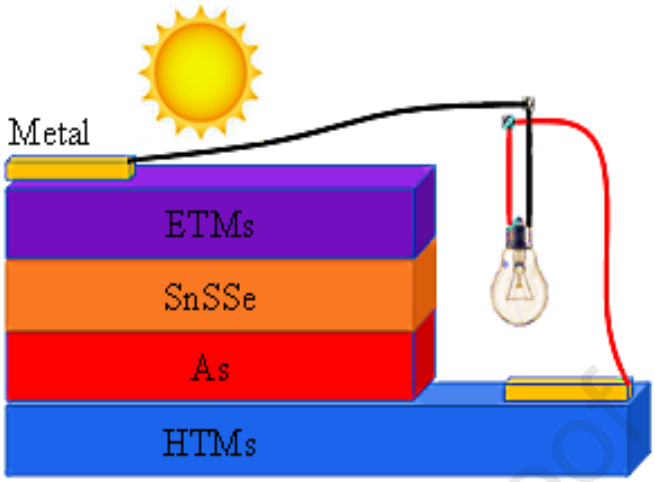

The designed photovoltaic device based on strain-tunable heterostructure

Achieving type-II SnSSe/As van der Waals heterostructure with satisfactory oxygen tolerance for optoelectronic and photovoltaic applications

Yee Hui Robin Chang [a, *], Junke Jiang [b], Keat Hoe Yeoh [c, d, *], Yusuf Zuntu Abdullahi [e, f], Heng Yen Khong [a], Moi Hua Tuh [g], Fui Kiew Liew [a], Yit Lian Liew [a]

[a] Faculty of Applied Sciences, Universiti Teknologi MARA, Cawangan Sarawak, 94300 Kota Samarahan, Sarawak, Malaysia
[b] Univ Rennes, ENSCR, CNRS, ISCR-UMR 6226, F-35000 Rennes, France
[c] Department of Electrical and Electronic Engineering, Lee Kong Chian Faculty of Engineering and Science, Universiti Tunku Abdul Rahman, 43000 Kajang, Selangor, Malaysia
[d] Center for Photonics and Advanced Material Research, Lee Kong Chian Faculty of Engineering and Science, Universiti Tunku Abdul Rahman, 43000 Kajang, Selangor, Malaysia
[e] Department of Physics, Faculty of Science, Kaduna State University, PMB 2339, Kaduna, Nigeria
[f] Department of Physics, Adnan Menderes University, Aydın 09010, Turkey
[g] Faculty of Computer & Mathematical Sciences, Universiti Teknologi MARA, Cawangan Sarawak, 94300 Kota Samarahan, Sarawak, Malaysia

[*] Electronic mail: robincyh@uitm.edu.my; keathoe.yeoh@gmail.com

Keywords: 2D heterostructure; Electronic structure; Optical absorption; Type-II band edge; Power conversion efficiency

Construction of van der Waals heterostructure provides a straightforward way to blend properties of different monolayer materials for enhanced photovoltaic performance. Herein, motivated by the successful characterization of monolayer SnX_2 (X = S, Se) and arsenene (As), detailed interfacial interaction and optical absorption proficiencies of novel SnSSe/As heterostructure have been systematically investigated. Findings reveal that the SnSSe/As heterostructure exhibits a type-II band arrangement with an indirect bandgap of 1.30 eV that approaches the desirable Shockley-Queisser Limit under 2% biaxial tensile strain, strong absorption of 10^4-10^5 cm^{-1} toward solar irradiation that encompasses the infrared-ultraviolet region and high carrier mobility up to 910.71 cm^2 V^{-1} s^{-1}. Large, negative binding energy and absence of chemical bonds at the heterostructure interface imply its stability. The dynamical and mechanical stabilities have also been confirmed. Moreover, analysis of oxygen adsorption suggests tolerable performance deterioration with SnSSe side facing the ambient air. Hence, a photovoltaic with power conversion efficiency (PCE) exceeding 30% is ultimately proposed.

1.0 Introduction

Lately, the energy demand has climbed sharply because of the rapid digitalization evolution for fulfilling global population lifestyle and ongoing industrial revolution. Due to the worsening energy overdraft and catalyzed environmental deterioration, development of durable and efficient photovoltaics is set to become a key element in the shift to renewable energy. The obligatory call for clean and renewable resources has prompted the need to explore durable and highly efficient photovoltaic materials. A preferred photovoltaic is typically characterized by high carrier mobility, environmental stability and wide energy range optical absorption. The groundbreaking discovery of graphene in its atomically thin form in 2004 marked the beginning of the age of 2D materials. However, the zero-bandgap semiconductor's small bandgap limited its usefulness. This has led researchers to focus on 2D materials that already possess semiconducting characteristics. Numerous studies have been conducted on 2D materials such as h-BN [1, 2], transition metal dichalcogenides (TMDC) [3-5], g-C3N4 [6] and MXene [7], owing to their intriguing electrical properties and controllable optical characteristics. Additionally, they can be synthesised into a wide range of nanomaterials with various potential gap and band position ranges to meet the potential requirements of a variety of photocatalytic reactions.

Van der Waals (vdW) heterostructures, which are constructed vertically utilising two or more distinct two-dimensional materials through weak vdW interactions, have recently gained popularity as a platform for the development of 2D materials. Very intriguingly, by carefully choosing the constituent materials, the band structure of the vdW heterostructures may form type-II band alignments in which photogenerated electron-hole pairs are successfully separated into two distinct layers, greatly slowing down the electron-hole recombination process and increasing the efficiency of solar cells. Hence, an attractive option for resolving the major energy and environmental problems that we are presently facing is the development of

materials with dual functions that can simultaneously meet both of these needs. The synthesis of heterostructure consisting of monolayer Janus transition metal dichalcogenide is made possible by the effective fabrication of Janus MoSSe and WSSe monolayers. The primary prepping techniques used in the synthesis include chemical vapour deposition (CVD), exfoliation and layer assembly, solution processing, and hydrothermal [8-11]. Materials made of monolayer SnX_2 (X = S, Se) have also been created [12, 13]. The Janus SnSSe monolayer might then be created by selenizing a SnS_2 monolayer or sulfurizing a $SnSe_2$ monolayer through the CVD process, following a similar technique to that used to create MoSSe. Since most of the identified Janus monolayers are also mechanically flexible in nature, deposition of a single layer indirect band gap material with exceptional carrier mobility, such as arsenene (As), onto the Janus monolayers may lead to improved performance and commerciality than their separate components, which have relatively larger band gaps. It was reported by Chang *et al* and Zhao *et al* [14, 15] that a series of solar cells may be constructed using 2D TMDC/As heterojunctions. In particular, $MoTe_2$/As [14] can reach PCE of 30.0 %.

To the best of our knowledge, the electronic and optical properties and related device applications of heterostructures consisting of monolayers SnSSe and As have not been studied thus far. In this study, the vdW heterostructure SnSSe/As has been proposed and built. Effects of biaxial strain and interlayer coupling towards band gap modulation of the heterostructure was also studied. Current findings show that the type-II band aligned SnSSe/As displays several interesting electronic characteristics, namely improved light absorption compared to its separate monolayer components and photoelectric power conversion efficiency (PCE) reaching 32%, which can be further enhanced under small tensile strain. Its more negative binding energy than that of bilayer graphene (-27.08 meV $atom^{-1}$) strongly indicates experimental synthesis possibility. Moreover, analysis of O adsorption suggests tolerable performance deterioration with SnSSe side facing the ambient air. This work elucidates the critical

significance of stacking in the utilisation of Janus SnSSe monolayer in renewable energy and laser protection, hence is expected to have far-reaching implications for the forecasting and enhancement of photoelectronic devices.

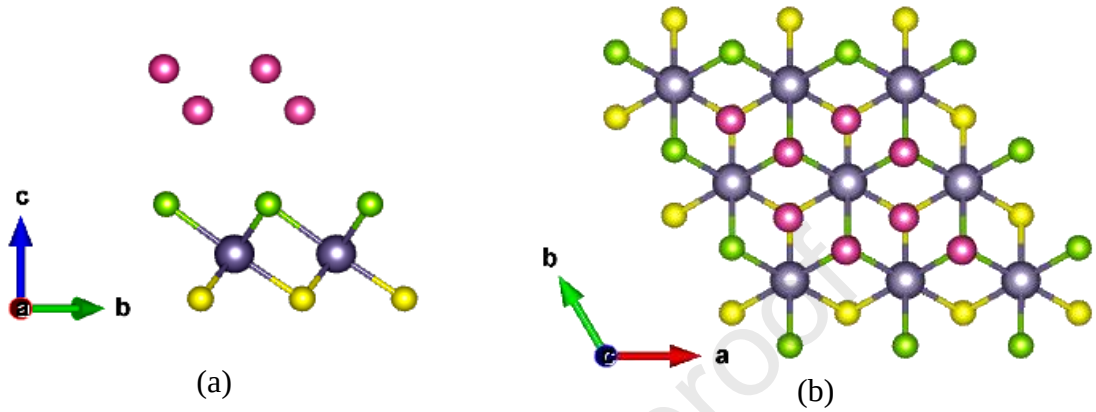

Figure 1 The (a) side and (b) top viewpoints of SnSSe/As vdW heterostructure. Grey, yellow, green and pink represents the Sn, S, Se and As atoms, respectively.

2.0 Computational methods

In current work, first-principles calculations based on density functional theory (DFT) were carried out by means of Vienna *Ab initio* Simulation Package (VASP) [16, 17], under the projector augmented wave (PAW) method with the exchange and correlation functional relations described by Perdew-Burke-Ernzerhof (PBE) [18]. During alternate structural relaxation between permissible ion position and volume (performed till within a single ionic step for both), the plane-wave cutoff, total energy convergence criterion, ionic force convergence and *k*-points grid were set to 450 eV, 10^{-5} eV, 10^{-3} eV Å^{-1} and 6 × 6 × 1, respectively. Allowing the volume to change would ensure the inclusion of positional selectivity. As ($3d^{10}4s^{2}4p^{3}$), Sn ($4d^{10}5s^{2}5p^{2}$), S ($3s^{2}3p^{4}$) and Se ($4s^{2}4p^{4}$) electron configurations were considered.

Adjacent layer spacing and electronic properties are significantly impacted by vdW forces. Hence, the long-range effect of vdW force was corrected using DFT-D3 approach of Grimme dispersion [19]. 30 Å vacuum was applied along the vertical direction to prevent interaction

between recurring images. For 2D materials, there are only two periodic directions, along x and y. Since the VASP package solves the Kohn-Sham equation within conventional 3D periodic boundary conditions, it is obligatory to add sufficient artificial vacuum space along the z-direction. For thermal stability check, *ab initio* molecular dynamics (AIMD) simulations were performed at 300 K up to 15 ps total simulation time using the Nose-Hoover thermostat [20]. To circumvent the underestimation of band gap by the use of PBE functional, the band gap magnitude of SnSSe/As and its constituent monolayers was recalculated using HSE06 [21] functional. The increment was added as scissor shift for optical calculations.

3.0 Results and discussion

3.1 Geometric stability and electronic properties

Before assembling the SnSSe/As heterostructure, atomic structures of the monolayers were first studied. The optimized lattice constant for SnSSe and As are 3.80 and 3.61 Å, respectively, showing close values with earlier reports [22, 23]. Their primitive cell is indicated by the hexagonal lattice class. Referring to **Figure 1**, the SnSSe/As heterostructure was then constructed by vertically stacking the structurally optimized monolayer As on monolayer SnSSe, forming a relaxed vdW heterostructure with lattice constant and interlayer distance of 3.69 and 3.09 Å, respectively. The lattice mismatch (δ), calculated using $\delta = 2(a_1 - a_2)/(a_1 + a_2)$, where a_1 and a_2 are the lattice constants of monolayers, is 5.1 %. This measurement is less than the critical limit of 8% while recent findings show that MoS_2/graphite and MoS_2/h-BN are experimentally achievable [24] despite having lattice mismatch exceeding 24%. To ensure the stability of the designed stacking, the interfacial binding energy (E_b) was evaluated to be -26.95 meV $Å^{-2}$ based on:

$$E_{\mathrm{b}} = \frac{E_{\mathrm{SnSSe/As}} - (E_{\mathbf{SnSSe}} + E_{\mathrm{As}})}{\mathrm{A}} \quad (1)$$

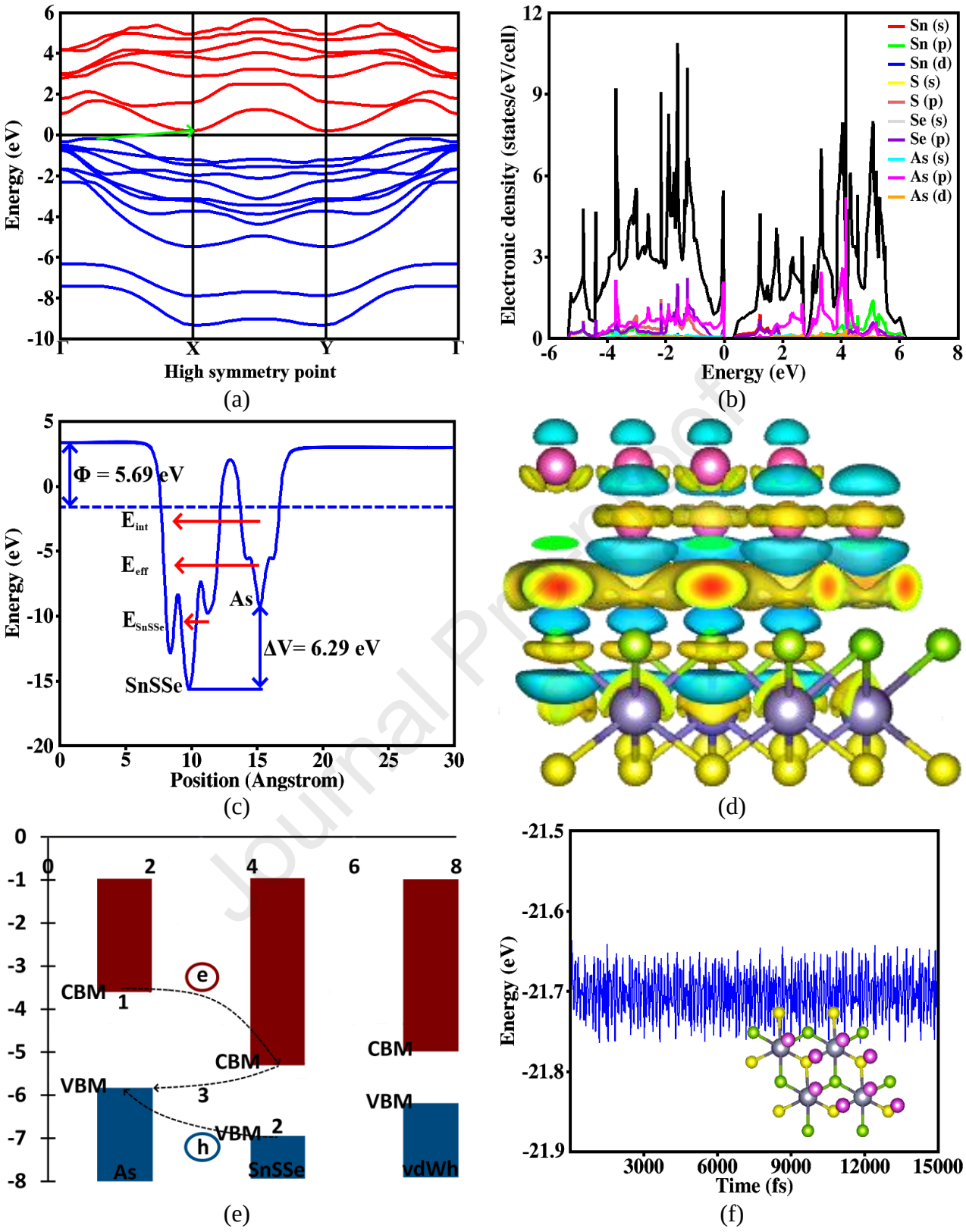

Figure 2 The (a) calculated band structure, (b) projected density of states (PDOS) at PBE level, (c) electrostatic potential in z-direction, (d) plane-averaged charge density difference, (e) band edge alignment for SnSSe/As heterostructure and (f) its total energy profile as a function of the *ab initio* molecular dynamic (AIMD) simulation step at 300 K.

where $E_{\mathrm{SnSSe/As}}$, E_{SnSSe}, E_{As} and A are the energies of SnSSe/As heterostructure, monolayer SnSSe, monolayer As and interface area, independently. The negative value means the heterostructure model is thermodynamically promising and in the typical vdW binding range.

Next, the projected band structure and density of states (PDOS) were calculated to provide a better insight towards the contribution of electronic orbitals accountable for the electronic behaviour, as shown in **Figure 2(a)** and **2(b)**. Findings indicate that SnSSe/As is an indirect band gap semiconductor with a measured interval of 1.30 eV at HSE06 level separating the valence band maximum (VBM) located along G-X direction and conduction band maximum (CBM) at X. The reduced band gap is conforming to current technological direction that entails a more extensive usage of medium and small band gap for better utilization of the visible portion of the solar spectrum. Detail analysis of the PDOS shows that the As 4*p* state is contributing heavily to the VBM, while the CBM is mainly composed of Sn 5*s* and Se 4*p* states, suggesting the formation of a type-II band alignment, which ultimately promotes electron-hole pair detachment and lower their recombination rate. To verify this, the charge transfer mechanism was probed via Bader charge analysis and charge density difference, obtained by $\Delta\rho = \rho_{\mathrm{SnSSe/As}} - (\rho_{\mathrm{SnSSe}} + \rho_{\mathrm{As}})$, where $\rho_{\mathrm{SnSSe/As}}$, ρ_{SnSSe} and ρ_{As} denotes the charge density of heterostructure and separate monolayers, individually.

The charge density plot in **Figure 2(d)** reveals charge depletion (blue region) in As layer while charge accretion (yellow region) near SnSSe layer, suggesting electrons transfer from As to SnSSe and consequently leading to deeper potential for SnSSe. The charge distribution is further confirmed by Bader charge analysis [25], in which the quantitative results point toward 0.015 |e| migration from As layer to SnSSe layer, generating an internal electric field (E_{int}) that acts in the same direction and further increases the movement of photo induced carriers, as displayed in **Figure 2(c)**. The small magnitude of transferred charge also implies the interaction between the monolayers is merely weak vdW at the interface. Due to the higher

electronegativity in S atoms compared to Se atoms, the atomic layer of S typically stores more electrons than the Se surface, thereby inducing an intrinsic electric field (E_{SnSSe}) that acts from Se atomic layer to S surface, raising the effective electric field (E_{eff}) and conclusively smoothing the charge transfer from As to SnSSe and promoting photocarrier separation.

These outcomes are also supported by the calculated work function (Φ), where As of lower Φ (5.42 eV) and SnSSe of greater Φ (6.38 eV) will physically act as p-doped and a n-doped materials, respectively. From mechanism viewpoint shown in **Figure 2(e)**, when exposed to light, the ① photoexcited electrons at CBM of As drift to CBM of SnSSe, while the ② induced holes at VBM of SnSSe travel to VBM of As. The ③ accumulated electrons at CBM of SnSSe then recombine with photogenerated holes at VBM of As. The first two processes are triggered by the conduction band offset (ΔV_{CBO}) and valence band offset (ΔV_{VBO}), causing the rapid separation of photogenerated carriers. The large offsets facilitate confinement of electrons and holes in the SnSSe and As monolayers. Due to the annihilation of photogenerated holes at VBM of As in the third process, there will be more photoinduced electrons (holes) than holes (electrons) in the As (SnSSe) layer, creating spatial separation of the photogenerated carriers. These observations suggest that the SnSSe/As heterostructure has the potential to be excellent photovoltaic materials. Typically, the phenomenon of quantum confinement in 2D materials broadens the band gap through elimination of *p* orbitals overlap. Hence, the enhanced *p* orbital interactions in SnSSe/As justifies the reduction in its band gap as compared to the monolayer SnSSe (1.72 eV) and As (2.29 eV). The aforementioned results demonstrate that the proposed heterojunction has an appropriate bandgap and properties that can effectively restrict the recombination of photogenerated carriers, hence satisfying the requirements for photovoltaic application.

Evidently in **Figure 2(f)**, the amplitude of total energy fluctuation as a function of AIMD simulation time is small, inferring sufficient thermal stability in SnSSe/As at room temperature.

Moreover, there is no evidence of substantial structure deformation or feature of broken bonds after 15 ps. Progressing to its mechanical behaviour, the calculated elastic coefficients $C_{11} \approx C_{22}$ = 138 N m^{-1}, C_{12} = 42 N m^{-1} and C_{66} = 45 N m^{-1} satisfy the C_{11} - $|C_{12}| > 0$ and $C_{66} > 0$ stability conditions, subsequently inferring sufficient mechanical stability in the investigated heterostructure. Poisson's ratio (υ) is another parameter that plays a crucial part in determining whether a material is ductile or brittle, since if $\upsilon > 0.26$, the material is ductile and otherwise brittle [26-29]. The resultant Young's modulus $E = (C_{11}C_{22} - C_{12}^2)/C_{11} = 125$ Nm^{-1} and $\upsilon = C_{12}/C_{11} = 0.30$ exemplify an improved stiffness compared to SnSSe but remains more flexible than graphene and other Janus heterostructure such as HfSSe/graphene [30].

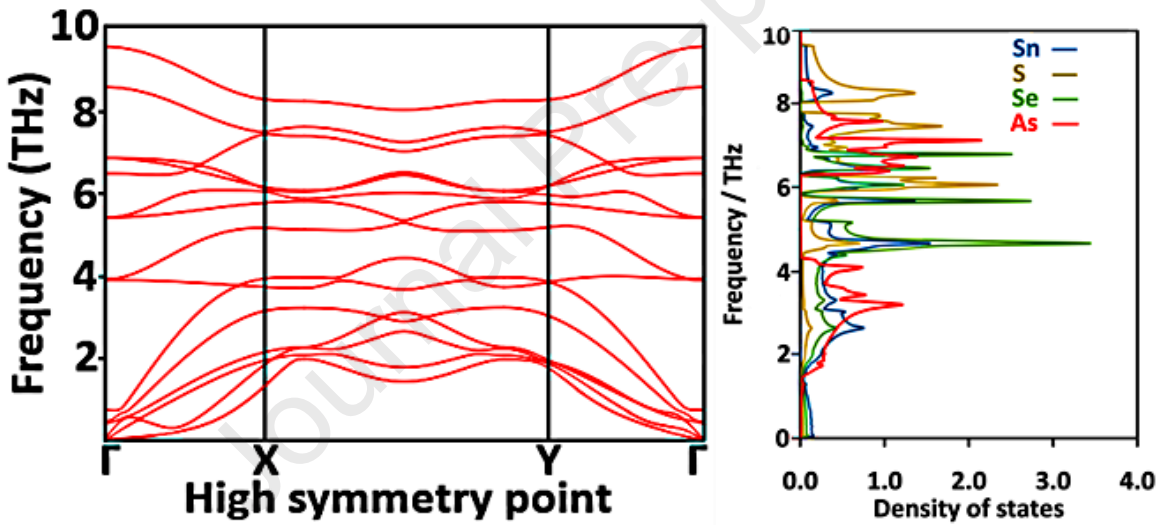

Figure 3 Calculated phonon dispersion spectra along high-symmetry points and phonon DOS for SnSSe/As heterostructure.

Figure 3 shows the calculated full phonon dispersion curves along high symmetry points within the Brillouin zone. The force constants were calculated by employing density generalized perturbation theory (DFPT) on 4 × 4 × 1 supercell, under strict convergence criteria of 10^{-8} eV. The phonon spectra were later generated by processing the atomic forces with the PHONOPY [31] code. The five atoms in the primitive cell constitutes 15 vibrational branches, with the heaviest Sn atom dominating the three acoustic branches while the highest lying

optical branches are contributed by the lightest S atom. As seen, there is no apparent feature of negative frequencies in the distribution, thus confirming the dynamical stability in the heterostructure.

3.2 Optoelectronic properties

Quantitative assessment on the competence to transfer carriers in specific direction is crucial for evaluating the optoelectronics performance of heterostructures. Due to the close proximity between acoustic phonon wavelength and electron coherence length, the use of deformation theory [32] for calculating intrinsic carrier mobility (μ) of inorganic materials is reasonable, as shown below.

$$\mu(\mathrm{2D}) = \frac{eC_{\mathrm{2D}}\hbar^3}{k_B T m^* m E_D^2} \tag{2}$$

in which e, C_{2D}, $\hbar$, k_B, T, m*, m and E_D signify the electron charge magnitude, direction bound elastic constant, reduced Planck constant, Boltzmann constant, surrounding temperature, average effective mass, effective mass in the direction of x or y and deformation potential constant (see Supplementary file **S1**), correspondingly.

Table 1 Calculated direction dependent effective mass m (m_0), E_D (eV), C_{2D} (N m^{-1}) and μ (cm^2 V^{-1} s^{-1}) for holes and electrons in the direction of x and y at 300 K. Relaxation time (τ) was estimated via $\tau = \mu m/e$. Exciton binding energy E_b^{ex} (eV) was calculated via $E_b^{ex} = 13.56(\mu/\varepsilon_0^2)$ where $\mu = \left(m_e^{-1} + m_h^{-1}\right)^{-1}$ and ε_0 denotes the reduced effective mass and static dielectric constant, respectively.

Heterostructure	Direction	Carrier type	m	E_D	C_{2D}	μ	τ	E_b^{ex}
SnSSe/As	x	Holes	0.800	2.12	138	910.71	4.14×10^{-13}	0.51
		Electrons	0.703	4.98		347.37	1.39×10^{-13}	
	y	Holes	1.007	1.90	138	900.76	5.16×10^{-13}	
		Electrons	0.335	5.19		671.16	1.28×10^{-13}	

Table 1 shows the calculated μ of SnSSe/As heterostructure at 300 K. The obtained μ for holes in the heterostructure is quite high, which is attributed to the insensitivity of the VBM

for strain, despite having effective mass larger than electrons. These measurements nevertheless are greater than or comparable to that of monolayer MoS_2 (200.52 $cm^2 V^{-1} s^{-1}$) [33], WS_2 (542.29 $cm^2 V^{-1} s^{-1}$) [34], BlueP (590 $cm^2 V^{-1} s^{-1}$) [35] and GaSe (866 $cm^2 V^{-1} s^{-1}$) [36]. In addition to the appropriate band gap, applicable band edge alignments and effective segregation of photogenerated carriers, the potential of materials as solar cell and water splitting photocatalyst is also depending on their optical absorption spectra α(ω), assessable via:

$$\alpha(\omega) = \sqrt{2}\omega \left[\sqrt{\varepsilon_1^2(\omega) + \varepsilon_2^2(\omega)} - \varepsilon_1(\omega)\right]^{\frac{1}{2}} \quad (3)$$

where $\varepsilon_1(\omega)$ and $\varepsilon_2(\omega)$ represent the real and imaginary components of dielectric function, while ω is the light frequency. The latter is computable via sum over a sufficiently large number of empty states. $\varepsilon_1(\omega)$ can then be realized from $\varepsilon_2(\omega)$ through Kramer-Kronig formulation.

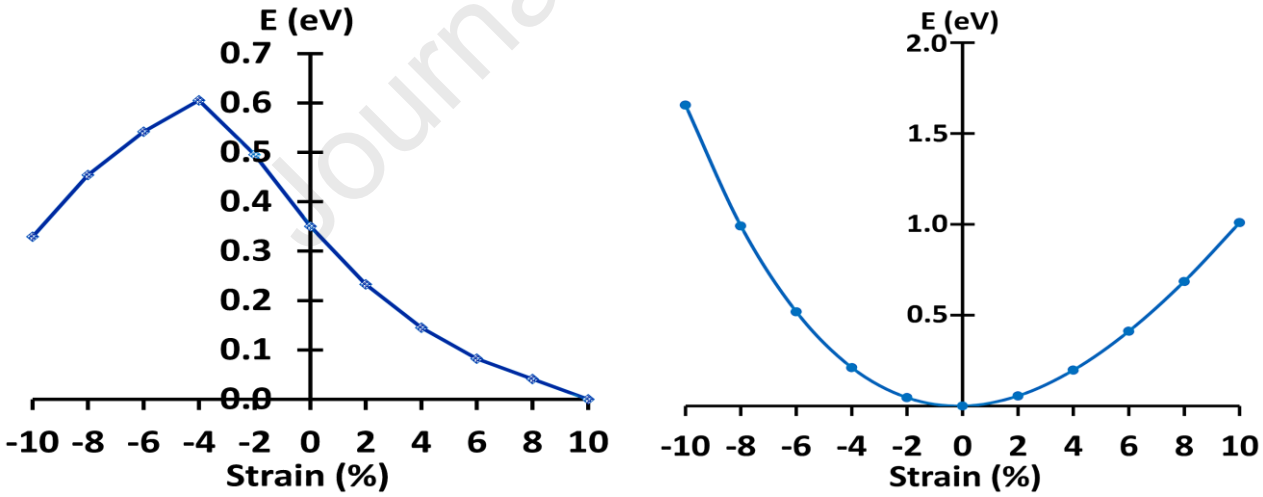

(a) (b)

Figure 4 (a) Band gap of SnSSe/As heterostructure at PBE level and (b) strain energy under various biaxial strains.

Given that visible light occupies 45% of the whole solar spectrum range, the capacity to absorb a significant portion of visible light is crucial. Interestingly, under biaxial strain, expressed as

$[(l - l_0)/l_0] \times 100\%$ where l and l_0 are the lattice constants before and after strained, it can be seen in **Figure 4(b)** that the curve profile is smooth and total energy of unstrained form is the lowest, inferring absence of phase transition and hence good stability. The positive and negative label exemplifies the tensile and compressive strains, correspondingly. Band gap variation under different biaxial strains is highlighted in **Figure 4(a)**. Overall, tensile strain causes the studied structure to undergo a consistent red shift whereas blue shift is noted for compressive strain till -4%, before switching to red shift under stronger compression. The former shifts the CBM downward greatly and the VBM downward marginally, leading to narrower bandgap, reducing from HSE06 corrected bad gap of 1.30 to 1.15 eV and 1.03 eV at 2% and 4% tensile strength, respectively, becoming much closer to the Shockley-Queisser (SQ) limit. In comparison to separated SnSSe and As layers, where the average α(ω) is below 0.5 × 10^5 cm^{-1} [37, 38], the SnSSe/As heterostructure presents a considerable red shift of light absorption edge, a steeper increase and substantially enhanced absorption intensity reaching 10^5 cm^{-1} order in the visible and near infrared domains, as shown in **Figure 5(a)**. Furthermore, the measured α(ω) of 10^4-10^5 cm^{-1} is comparable to several conventional photovoltaics such as c-Si, Ge, GaAs, InP [39] and Rb-based compounds [40-42], strengthening its credibility as potential high performance photovoltaic. Formation of SnSSe/As heterostructure creates more energy bands and raises the hybridization-based joint density of states near the VBM, which significantly increases the interband transition probability of electrons from As *p* states in the valence band to Sn *s* and Se *p* states of the conduction band.

To delve into the ability of SnSSe/As in harvesting solar energy, the spectroscopic limited maximum efficiency (SLME) has been evaluated. This model [43, 44] provides a quantifiable selection metric to screen photovoltaic efficiencies of materials through the integration of their band gap energies, absorption spectra and non-radiative recombination losses relating to typical

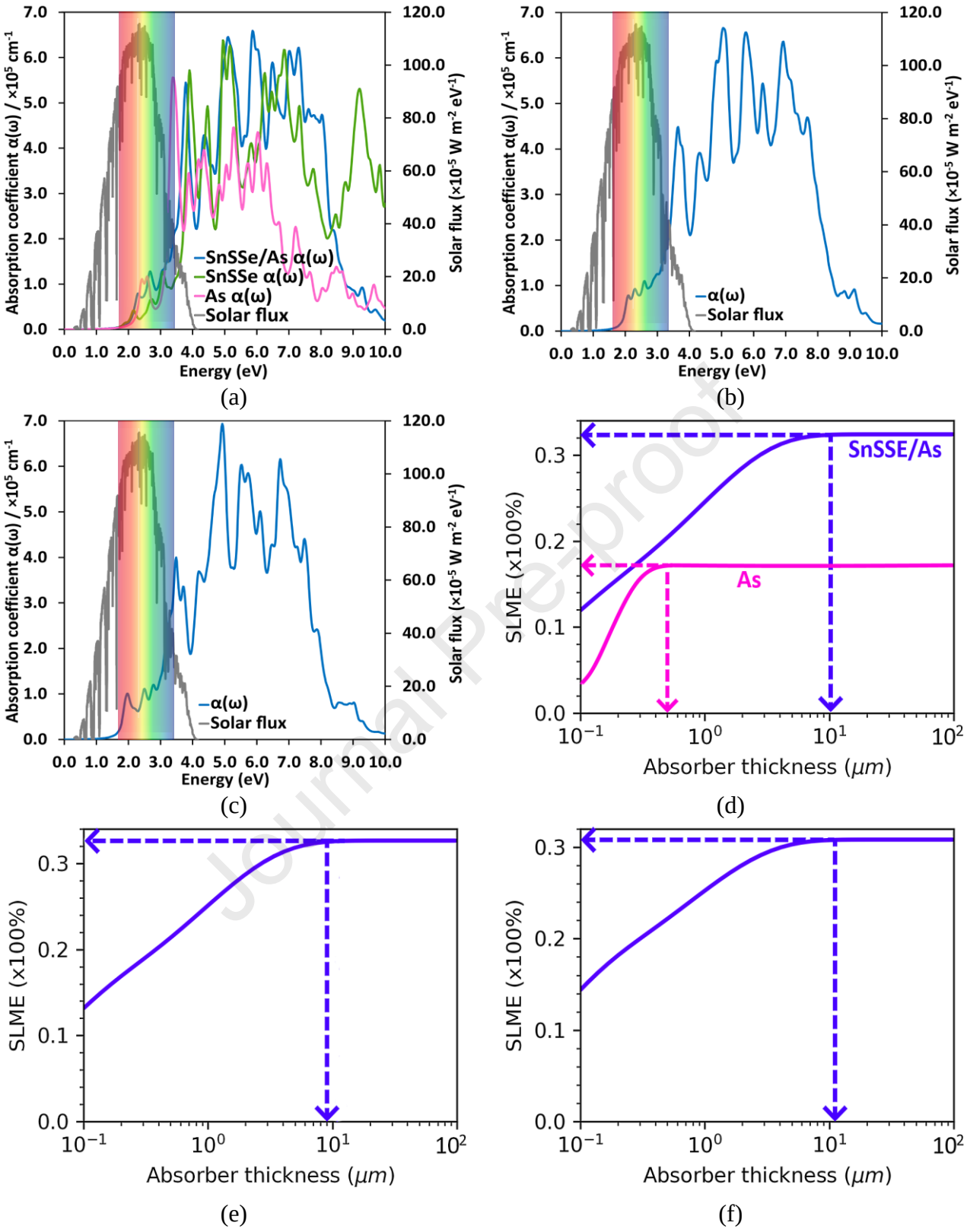

Figure 5 Absorption coefficients α(ω) for SnSSe/As (a) in the absence of biaxial strain, (b) under 2% tensile strain and (c) under 4% tensile strain, calculated by DFT+BSE with scissor approach. (d, e and f) are their respective SLME (see Supporting Information **S2** for calculation details), as the function of film thickness ranging from 0.1 to 100 μm.

Air Mass 1.5G (AM1.5G) solar energy flux or P(ω), subsequently showing relevance to real-time applications by expanding the traditional SQ limit. As illustrated in **Figure 5(b)**, red shift induced by 2% tensile strain produces more absorption peaks in visible light region and increases the effective light absorption, where a broader and more consistent overlap (from 2.0 to 3.5 eV) with incident AM1.5G solar flux is observed, finally raising the SLME to ~14%at ultrathin 0.1 μm thickness and reaching the ~33% saturation level at reduced thickness. Further red shift with reduced α(ω) near the solar flux peak is detected under 4% tensile strain, resulting in a lower SLME due to larger band gap shift from the 1.1 eV SQ limit but attaining higher SLME ~ 15% at 0.1 μm thickness. On a side note, materials with high α(ω) may also be applied as absorber shield. For instance, a YAG laser of wavelength 1064 nm is employed in various significant applications, including the cutting of materials [45] and the delivery of medications [46]. However, a previous study found that exposure to picosecond Nd:YAG laser pulses could harm the eyes [47]. In order for laser technology to be widely used, it is crucial that people are protected from harmful laser irradiation. The quest for materials that can shield people from harmful incident laser beams are therefore crucial. As pointed out in **Figure 5(a)**, although pure arsenene can be utilized as a shielding material, SnSSe heterostructure owing to the higher α(ω) over broader spectral range provides better defense against laser beams in the ultraviolet, visible and near infrared ranges, making it a promising shield against any source of undesired laser radiation as a result. This observation is also supported by **Figure 5(d)**, in which the SLME for SnSSe/As is almost twice that of As at saturation level.

3.3 Impact of O adatoms on photovoltaic performance

In actual application, when exposed to surrounding air, electrical performance and durability of photovoltaic will be impacted by the contamination of active layer by O atoms. Following studies were performed on the basis that the adsorption of O atoms with the studied heterostructure is ascribed to surface adsorption, thus only interact with the top surface layer.

Taking these into considerations, the effect of O adsorption on the band structure of OSnSSe/As (adsorption on SnSSe side) and SnSSe/AsO (adsorption on As surface) heterostructures were additionally carried out. The analogous band structures in **Figures 6(a)** and **6(b)** suggest that O atoms adsorption launches impurity states and alters the electronic properties considerably, where the CBM for SnSSe/AsO and OSnSSe/As is shifted from X to Y and X to Γ points, respectively, due to band folding. SnSSe/AsO is affected more by the impurity states, as evident

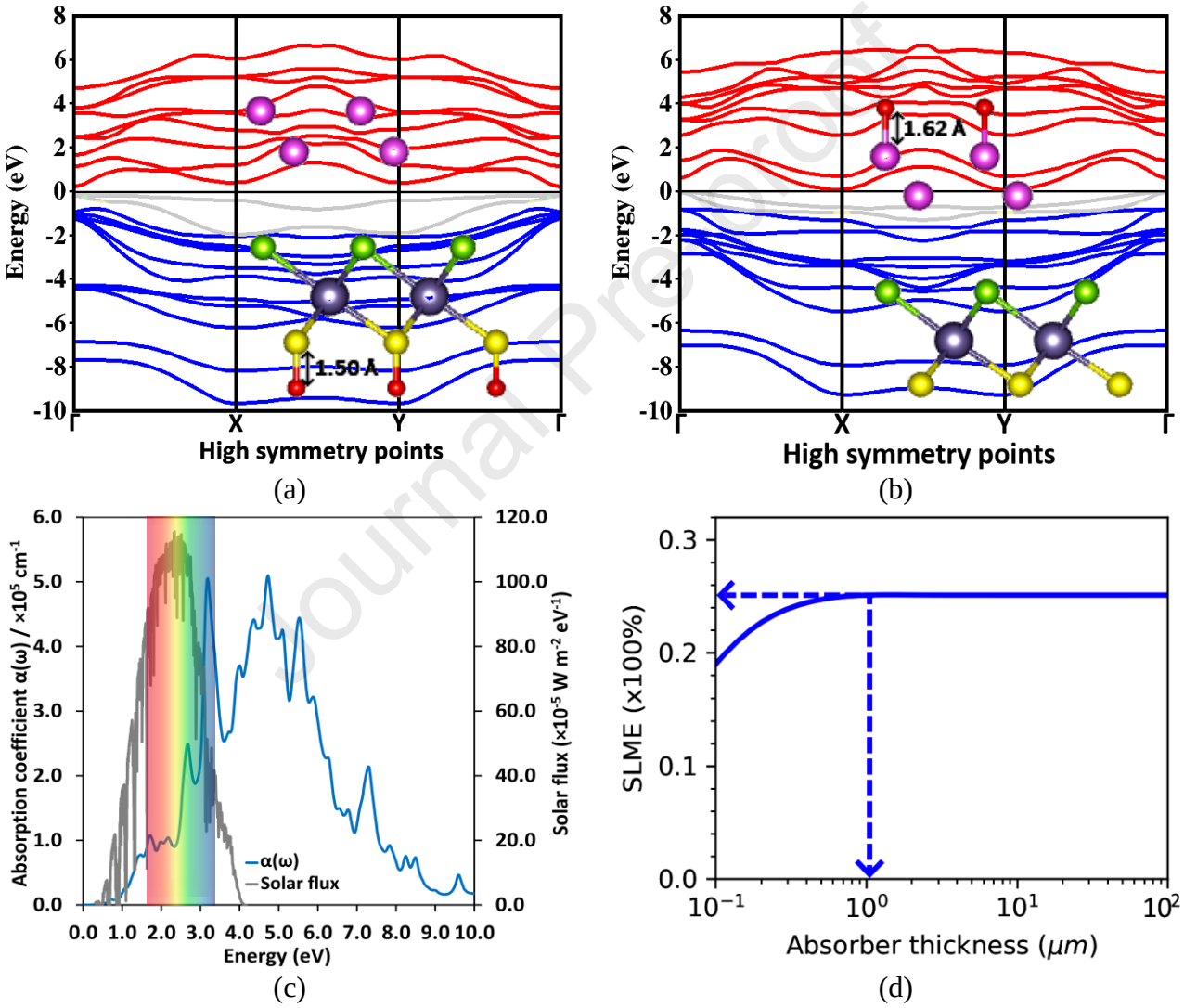

Figure 6 Projected band structure plot for (a) OSnSSe/As and (b) SnSSe/AsO heterostructures, at PBE level. Grey lines are contributions from O adatoms (indicated by red circle) based on 2 × 2 supercell. (c) Absorption coefficients α(ω) and (d) thickness dependence of SLME for O atom adsorbed on SnSSe surface of the heterostructure, labelled as OSnSSe/As.

by the obvious greater band gap reduction and conductive transformation. While the adsorption of O atoms on SnSSe side produces perceptible alteration on the states near VBM, the band gap does not suffer from drastic changes, decreasing moderately to 0.82 eV at HSE06 level and attaining a relatively high SLME of 25% at remarkably thin absorber layer of 1.0 μm, as shown in **Figures 6(c)** and **6(d)**. Adsorption energy was additionally calculated to provide a quantitative clarification on this phenomenon. The stability between the adsorbent (SnSSe/As) and the adsorbate (O) is assessed and described by the adsorption energy (E_{ads}), expressed as follows:

$$E_{\mathrm{ads}} = E_{\mathrm{SnSSe-As/O}} - (E_{\mathrm{SnSSe-As}} + E_{\mathrm{O}}) \quad (4)$$

where $E_{\mathrm{SnSSe\text{-}As}}$ and E_{O} indicates the total ground state energy of heterostructure and O atom before occurrence of adsorption, respectively, and $E_{\mathrm{SnSSe\text{-}As/O}}$ indicates the total ground state energy of O adsorbed SnSSe/As. One of the two possible modes of adsorption operation is physisorption, which depends on weak vdW interactions between the interacting species. Electrical characteristics of adsorbent is hardly affected through this method. In contrast, perturbation of electronic system tends to be greater in chemisorption, the second mode which is activated via strong covalent bonding between interacting species. Calculated E_{ads} for OSnSSe/As and SnSSe/AsO is -4.81 and -5.13 eV, correspondingly. The higher E_{ads} for SnSSe/AsO suggests stronger chemisorptive nature. This assumption is also explainable by the shorter As-O bond length (1.62 Å) compared to its actual average length of 1.77 Å, while photovoltaic performance will be less affected with SnSSe side facing the ambient air because S-O bond length in OSnSSe/As (1.50 Å) appears elongated compared to actual S-O bond length (1.43 Å). In addition, AIMD simulation in **Figure 7(a)** indicates that OSnSSe/As is still stable after 15 ps annealing and its resultant S-O bond length of 1.47 Å remains stretched out. These findings imply that while the performance of SnSSe/As deteriorates when it is exposed to

ambient air, the deterioration can be minimized by aligning the SnSSe surface as the exterior side. On a positive note, the contaminated heterostructure is still able to achieve reasonable maximum efficiency at significantly lower absorber thickness.

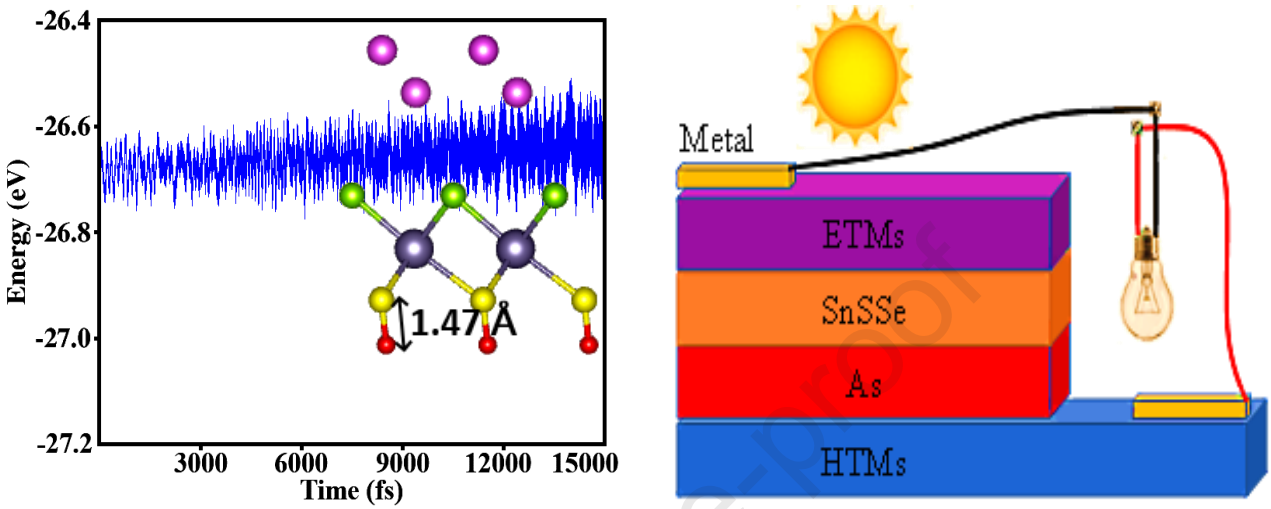

(a) (b)

Figure 7 (a) AIMD simulation of OSnSSe/As and (b) the proposed heterostructure-based solar cell arrangement.

Hence, a high SLME heterostructure-based photovoltaic cell with SnSSe side facing the air is proposed, as demonstrated in **Figure 7(b)**, where HTM (such as spiro-OMeTAD) refers to hole transport material, while ETM (commonly anatase) is the electron transport material. Apart from acting as supporting substrates for SnSSe/As heterostructure, both HTM and ETM also play important roles by extracting holes and electrons, simultaneously, therefore decreases charge recombination. Under light irradiation, the SnSSe/As heterostructure within the device will absorb the incoming photons and initiate sequence of electron transition. The photogenerated carriers are effectively isolated across the monolayers due to the type-II nature of SnSSe/As, thus inducing a photovoltaic voltage required for supplying current to the external devices. Based on these findings, we can infer that the performance of heterostructure-based devices will be diminished when exposed to ambient air. Thus, the present investigation into

how to prevent the adsorption of O atoms on the technologies is a useful undertaking for their practical application.

4.0 Conclusion

The interfacial, electronic, mechanical, dispersion relation and optical properties of novel SnSSe/As heterostructure have been systematically investigated, based on first principles DFT calculations with vdW correction. The optimized configuration is a type-II semiconductor that demonstrates structural, mechanical and dynamical stabilities, as verified by the negative binding energy, small lattice mismatch, Born-Huang stability criteria adherence, AIMD simulation and phonon spectra analyses. The measured E_b of -26.95 meV $Å^{-2}$ is comparable to several typical vdW bonded materials, namely graphite (-12 meV $Å^{-2}$), bulk MoS_2 (-26 meV $Å^{-2}$) and $MoTe_2/SnSe_2$ (-15 meV $Å^{-2}$), hence confirming the long-range vdW forces influence on interfacial properties of SnSSe/As heterostructure. As a result of the enhanced *p* orbital interaction, which reduces the electronic band gap, the studied heterostructure undergoes red shift of absorption edge with respect to its monolayer constituents, hence effectively raising the α(ω) in visible region. Biaxial strain can effectively modulate its band gap, with no change in band alignment type observed. Under 2% tensile strain, the SLME improved to a record high ~33%. Moreover, deterioration in performance when the heterostructure is exposed to ambient air can be reduced by positioning SnSSe as top layer. To boost the stability of the material class, affordable encapsulation techniques and oxygen-resistant additives can be considered in future studies. Overall, the high α(ω), superior PCE and impressive oxygen tolerance demonstrated by the studied heterostructure suggest its suitability as energy-harvesting materials. Our results should therefore encourage further experimental work toward the synthesis and thermal transport characterization of Janus SnSSe monolayers, in addition to unveiling its potential for application in optoelectronics and nanoelectronics devices.

CRediT authorship contribution statement

Y.H.R. Chang: Conceptualization, Methodology, Software, Formal analysis, Investigation, Data curation, Project administration, Writing - original draft. J. Jiang, K.H. Yeoh: Software, Formal analysis, Investigation, Validation, Resources, Writing - review & editing. H.Y. Khong, Y.Z. Abdullahi, M.H. Tuh, F.K. Liew, Y.L. Liew: Validation, Visualization, Writing - review & editing.

Declaration of competing interest

The authors declare that they have no known competing financial or personal interests.

References

[1] C. Yu, J. Zhang, W. Tian, X. Fan, Y. Yao (2018). Polymer composites based on hexagonal boron nitride and their application in thermally conductive composites. *RSC Adv.*, 8, 21948-21967.

[2] J. Ren, P. Innocenzi (2021). 2D Boron Nitride Heterostructures: Recent Advances and Future Challenges. Small Structures, 2, 11, 2100068.

[3] Y.H.R. Chang, J. Jiang, H.Y. Khong, I. Saad, S.S. Chai, M.M Mahat, S. Tao (2021). Stretchable AgX (X = Se, Te) for Efficient Thermoelectrics and Photovoltaics. *ACS Appl. Mater. Interfaces*, 13, 25121-25136.

[4] Y.H.R. Chang (2020). High mechanical strength and broad optical absorption in underexplored group IV nitride chalcogenides. *Chem. Commun.*, 56, 74, 10962-10965.

[5] G. Wang, C. Chen, B.S. Teketel, B. Xu, B. Lin (2021). Constructing a new 2D Janus black phosphorus/SMoSe heterostructure for spontaneous wide-spectral-responsive photocatalytic overall water splitting. International Journal of Hydrogen Energy, 46, 79, 39183-39194.

[6] S. Cao, J. Low, J. Yu, M. Jaroniec (2015). Polymeric photocatalysts based on graphitic carbon nitride. *Adv. Mater.*, 27, 2150-2176.

[7] A. Bhat, S. Anwer, K.S. Bhat, M.I.H. Mohideen, K. Liao, A. Qurashi (2021). Prospects challenges and stability of 2D MXenes for clean energy conversion and storage applications. npj 2D Materials and Applications, 5, 61.

[8] J. Azadmanjiri, V.K. Srivastava, P. Kumar, Z. Sofer, J. Min, J. Gong (2020). Graphene-Supported 2D transition metal dichalcogenide van der waals heterostructures. *Appl. Mater. Today* 19, 100600.

[9] Y.-C. Lin, C. Liu, Y. Yu, E. Zarkadoula, M. Yoon, A.A. Puretzky, L. Liang, X. Kong, Y. Gu, A. Strasser, H.M. Meyer III, M. Lorenz, M.F. Chisholm, I.N. Ivanov, C.M. Rouleau, G. Duscher, K. Xiao, D.B. Geohegan (2020). Low Energy Implantation into Transition-Metal Dichalcogenide Monolayers to Form Janus Structures. *ACS Nano,* 14, 4, 3896-3906.

[10] A.-Y. Lu, H. Zhu, J. Xiao, C.-P. Chuu, Y. Han, M.-H. Chiu, C.-C. Cheng, C.-W. Yang, K.-H. Wei, Y. Yang, Y. Wang, D. Sokaras, D. Nordlund, P. Yang, D.A. Muller, M.-Y. Chou, X. Zhang, L.-J. Li (2017). Janus monolayers of transition metal dichalcogenides. Nature Nanotechnology 12, 744-749.

[11] J. Zhang, S. Jia, I. Kholmanov, L. Dong, D. Er, W. Chen, H. Guo, Z. Jin, V.B. Shenoy, L. Shi, J. Lou (2017). Janus Monolayer Transition-Metal Dichalcogenides. *ACS Nano,* 11, 8, 8192-8198.

[12] X. Zhou, L. Gan, W. Tian, Q. Zhang, S. Jin, H. Li, Y. Bando, D. Golberg, T. Zhai (2015). Ultrathin $SnSe_2$ Flakes Grown by Chemical Vapor Deposition for High-Performance Photodetectors. Advanced Materials 27, 48, 8035-8041.

[13] X. Zhou, Qi Zhang, L. Gan, H. Li, T. Zhai (2016). Large-Size Growth of Ultrathin SnS_2 Nanosheets and High Performance for Phototransistors. Advanced Functional Materials 26, 24, 4405-4413.

[14] Y.H.R Chang, K.H. Yeoh, J. Jiang, T.L. Lim, Y.S. Yong, L.C. Low, M.H. Tuh (2022). Constructing trifunctional $MoTe_2$/As van der Waals heterostructures for versatile energy applications. *New J. Chem.*, 46, 20172-20181.

[15] H. Zhao, F. Xie, Y. Liu, B. Bian, G. Yang, Y. Ding, Y. Gu, Y. Yu, X. Zhang, X. Huo, B. Hua, X. Ni, Q. Fan, X. Gu (2021). Van der Waals heterostructures of Janus XSeTe (X = Mo, W) and arsenene monolayers: A first principles study. Materials Science in Semiconductor Processing, 123, 105588.

[16] G. Kresse, J. Furthmüller (1996). Efficient Iterative Schemes for *Ab initio* Total-energy Calculations Using a Plane-wave Basis Set. *Phys. Rev. B* 54, 11169.

[17] G. Kresse, J. Furthmüller (1996). Efficiency of *Ab-initio* Total Energy Calculations for Metals and Semiconductors Using a Plane-wave Basis Set. *Comput. Mat. Sci.*, 6, 15-50.

[18] J.P. Perdew, K. Burke, M. Ernzerhof (1996). Generalized Gradient Approximation Made Simple. *Phys. Rev. Lett.*, 77, 3865-3868.

[19] S. Grimme, J. Antony, S. Ehrlich, H. Krieg (2010). A consistent and accurate ab initio parametrization of density functional dispersion correction (DFT-D) for the 94 elements H-Pu. *J. Chem. Phys.* 132, 154104.

[20] S. Nosé (1984). A Unified Formulation of The Constant Temperature Molecular Dynamics Methods. *J. Chem. Phys.* 81, 511.

[21] J. Heyd, G.E. Scuseria (2004). Efficient hybrid density functional calculations in solids: Assessment of the Heyd-Scuseria-Ernzerhof screened Coulomb hybrid functional. *J. Chem. Phys.*, 121 (3), 1187-1192.

[22] S. Zhang, Z. Yan, Y. Li, Z. Chen, H. Zeng (2015). Atomically thin arsenene and antimonene: semimetal-semiconductor and indirect-direct band-gap transitions. *Angew. Chem. Int. Ed. Engl.* 54, 3112-3115.

[23] Y.H.R. Chang, T.L. Yoon, K.H. Yeoh, T.L. Lim (2021). Integrated SnSSe bulk and monolayer as industrial waste heat thermoelectric materials. *Int. J. Energy Res.*, 45, 2, 2085-2099.

[24] M. Liao, P. Nicolini, L. Du, J. Yuan, S. Wang, H. Yu, J. Tang, P. Cheng, K. Watanabe, T. Taniguchi, L. Gu, V.E.P. Claerbout, A. Silva, D. Kramer, T. Polcar, R. Yang, D. Shi, G. Zhang (2022). UItra-low friction and edge-pinning effect in large-lattice-mismatch van der Waals heterostructures. Nature Materials 21, 47-53.

[25] W. Tang, E. Sanville, G. Henkelman (2009). A grid-based Bader analysis algorithm without lattice bias, *J. Phys.: Condens. Matter*, 21, 084204.

[26] G.M. Mustafa, S. Saba, N.A. Noor, A. Laref, M. Abd El-Rahman, Z. Farooq, R.B. Behram, Z. Ullah (2023). First-principles calculations to investigate HgY_2S/Se_4 spinel chalcogenides for optoelectronic and thermoelectric applications. Journal of Materials Research and Technology 22, 97-106.

[27] N.A. Noor, M. Rashid, G.M. Mustafa, A. Mahmood, W. Al-Masry, S.M. Ramay (2021). Zinc based chalcogenides $ZnMn_2X_4$ (X = S, Se, Te) as promising spintronic and sustainable energy materials: Ab-initio DFT investigations. Journal of Alloys and Compounds 856, 157198.

[28] T. Alshahrani, G.M. Mustafa, T.H. Flemban, H. Althib, S. Al-Qaisi, N.A. Kattan, Q. Mahmood (2020). Probing of Optoelectronic and Transport Properties of Zinc Based ZnY_2X_4 (X = S, Se) Spinels for Renewable Energy. *ECS J. Solid State Sci. Technol.*, 9, 105001.

[29] G.M. Mustafa, T. Zelai, S. Bouzgarrou, M.H. Alhossainy, Q. Mahmood, A. Mera, H.H. Hegazy, S. Alharthi, M.A. Amin (2022). First principle study of magnesium-based chalcogenides $MgLa_2(S/Se)_4$ for solar cells and renewable energy applications. Applied Physics A, 128, 38.

[30] Q. Luo, S. Yin, X. Sun, G. Guo, X. Dai (2022). Interlayer coupling and external electric field controllable electronic structures and Schottky contact of HfSeX (X = S, Se)/graphene van der Waals heterostructures. Diamond & Related Materials 128, 109223.

[31] L. Chaput, A. Togo, I. Tanaka, G. Hug (2011). Phonon-phonon interactions in transition metals. *Phys. Rev. B: Condens. Mater. Phys.* 84, 094302-094306.

[32] J. Bardeen, W. Shockley (1950). Deformation Potentials and Mobilities in Non-Polar Crystals. *Phys. Rev.*, 80, 1, 72-80.

[33] Y. Cai, G. Zhang, Y.W. Zhang (2014). Polarity-Reversed Robust Carrier Mobility in Monolayer MoS2 Nanoribbons. *J. Am. Chem. Soc.*, 136, 6269-6275.

[34] R. Kumar, D. Das, A.K. Singh (2018). C_2N/WS_2 van der Waals type-II heterostructure as a promising water splitting photocatalyst. *J. Catal.*, 359, 143-150.

[35] J. Xiao, M. Long, C.-S. Deng, J. He, L.-L. Cui, H. Xu (2016). Electronic Structures and Carrier Mobilities of Blue Phosphorus Nanoribbons and Nanotubes: A First-Principles Study. *J. Phys. Chem. C*, 120, 4638-4646.

[36] Yu Cui, Lei Peng, Liping Sun, Qi Qian, Yucheng Huang (2018). Two-dimensional few-layer group-III metal monochalcogenides as effective photocatalysts for overall water splitting in the visible range. *J. Mater. Chem. A*, 6, 22768-22777.

[37] M. Sun, J.-P. Chou, J. Gao, Y. Cheng, A. Hu, W. Tang, G. Zhang (2018). Exceptional Optical Absorption of Buckled Arsenene Covering a Broad Spectral Range by Molecular Doping. *ACS Omega*, 3, 8514-8520.

[38] Marwan Alam, Hafiza Sumaira Waheed, Hamid Ullah, M. Waqas Iqbal, Young-Han Shin, Muhammad Junaid Iqbal Khan, H.I. Elsaeedy, R. Neffati (2022). Optoelectronics properties of Janus SnSSe monolayer for solar cells applications. *Phys. B: Condensed Matter*, 625, 413487.

[39] I. Massiot, A. Cattoni, S. Collin (2020). Progress and prospects for ultrathin solar cells. *Nature Energy* 5, 959-972.

[40] Q. Mahmood, G.M. Mustafa, N.A. Kattan, T. Alshahrani, N. Sfina, A. Mera, Z.H. Shah, H.H. Somaily, S. Alharthi, M.A. Amin (2022). Tunning of band gap of double perovskites halides Rb_2CuSbX_6 (X = Cl, Br, I) for solar cells and energy harvesting. Materials Science and Engineering: B, 286, 116088.

[41] P.A. Nawaz, G.M. Mustafa, S.S. Iqbal, N.A. Noor, T.S. Ahmad, A. Mahmood, R. Neffati (2022). Theoretical investigations of optoelectronic and transport properties of Rb_2YInX_6 (X = Cl, Br, I) double perovskite materials for solar cell applications. Solar Energy, 231, 586-592.

[42] A. Ul Haq, G.M. Mustafa, M. Amin, S.M. Ramay, A. Mahmood (2021). Ab-initio study of opto-electronic and thermoelectric properties of direct bandgap double perovskites Rb_2XGaBr_6 (X = Na, K). International Journal of Energy Research, 45, 6, 9241-9251.

[43] L. Yu, A. Zunger (2012). Identification of Potential Photovoltaic Absorbers Based on First-Principles Spectroscopic Screening of Materials. *Phys. Rev. Lett.*, 108, 068701.

[44] Y.H.R. Chang, J. Jiang, K.H. Yeoh, H.Y. Khong, M.M. Mahat, S.S. Chai, I. Saad, M.H. Tuh (2022). Improved Thermoelectric-Photovoltaic Performance of Ag_2Se Originating from a Halogenation-Induced Wider Band Gap and Low Crystal Symmetry. *ACS Appl. Energy Mater.*, 5, 6019-6031.

[45] A. Sharma, V. Yadava (2018). Experimental analysis of Nd-YAG laser cutting of sheet materials - A review. Optics & Laser Technology 98, 264-280.

[46] L.R. Sklar, C.T. Burnett, J.S. Waibel, R.L. Moy, D.M. Ozog (). Laser assisted drug delivery: A review of an evolving technology. *Lasers Surg. Med.*, 46, 249-262.

[47] W.T. Ham, H.A. Mueller, A.I. Goldman, B.E. Newnam, L.M. Holland, T. Kuwabara (1974). Ocular Hazard from Picosecond Pulses of Nd: YAG Laser Radiation. Science, 185, 362-363.

Highlights

- Novel vdW SnSSe/As heterostructures are potential candidate for solar energy material.
- The band edges analysis reveals a type-II heterostructure for each system.
- Absorption coefficient of 10^5 cm^{-1} was attained within the infrared-ultraviolet range.
- They fulfil the requirements of ~30% solar to electricity conversion efficiency.
- Improved oxygen tolerance when SnSSe side is exposed to ambient air.

Declaration of Interest Statement

The authors declare that they have no known competing financial or personal interests.